ACS OMEGA

http://pubs.acs.org/journal/acsodf

Article

Bismuth and Vanadium-Substituted Yttrium Phosphates for Cool Coating Applications

Vasudevan Elakkiya and Shanmugam Sumathi*

Cite This: *ACS Omega* 2022, 7, 44266−44277

Read Online

ACCESS | Metrics & More | Article Recommendations

ABSTRACT: Luminescent yttrium phosphate is engineered into an environmentally benign near infrared (NIR) reflective yellow pigment by the substitution of bismuth and vanadium metals in the host lattice. A series of $YP_{(1-x)}V_xO_4$ (x = 0, 0.05, 0.1, 0.15, 0.2, and 0.4), $Y_{(1-y)}Bi_yPO_4$ (y = 0.1 and 0.3), and $Y_{(1-y)}Bi_yP_{(1-x)}V_xO_4$ ($x = y$ = 0.2, 0.4, and 0.6) were prepared by the precipitation method. Secondary phase was noticed at x = 0.2 and y = 0.2 while substituting vanadium and bismuth, respectively, due to high ionic radii of the dopant ions. Co substitution of vanadium and bismuth in the YPO_4 lattice enhanced both NIR reflectance and yellow color of all the fabricated materials. XPS spectra proved the presence of trivalent bismuth and pentavalent vanadium in $Y_{0.4}Bi_{0.6}P_{0.4}V_{0.6}O_4$. Due to the substitution effect, a more defined morphology was noticed, which enhanced the scattering co-efficient of the fabricated materials; hence, the NIR reflectance of the materials was increased from 68% (YPO_4) to 83% ($Y_{0.4}Bi_{0.6}P_{0.4}V_{0.6}O_4$). Chemical and thermal stability test of $Y_{0.4}Bi_{0.6}P_{0.4}V_{0.6}O_4$ confirmed the color and strength of the designed pigment. With good yellow hue (b^* = +56.06), high NIR solar reflectance (R^* = 83%), and good stability, $Y_{0.4}Bi_{0.6}P_{0.4}V_{0.6}O_4$ can act as an environmentally benign cool yellow pigment.

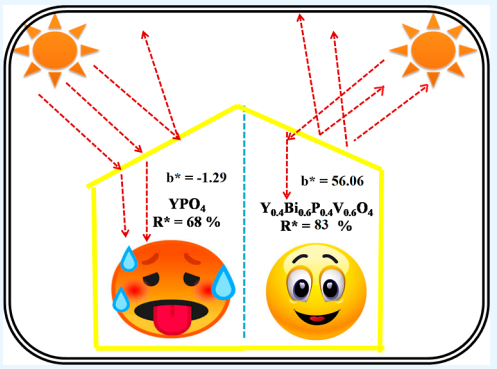

1. INTRODUCTION

The urban heat island (UHI) effect is one of the most serious discomforts experienced by the people who live in cities. Due to this effect, the interior of the built up area experiences more heat than its external surroundings. The UHI effect is generally caused due to the absorption of solar radiation by the buildings and other architectures in the urban areas during the long day time, and no dissipation of the absorbed energy in the night time.[1] This phenomenon significantly increases the difference in temperature between urban and rural areas (the radiation is more rapid due to natural greeneries). In order to reduce the high interior temperature, use of air conditioners are preferred which consumes around 40% of electricity.[2] Heat absorption is quite high when the buildings are made of asphalt sheets, cement, concretes, and metallic structures.[3] Since approximately 53% of the solar radiation consists of the near-infrared region (NIR), it is obvious that building infrastructures coated with NIR-reflective materials could effectively reduce the interior temperature, in turn keeping the building cool. Hence, these NIR-reflective materials are coined as cool coating materials.[4]

Neoteric investigators are focused on the synthesis of NIR reflective materials based on rare earth materials as host/dopant compound; hence one could increase the reflectivity of the material while maintaining the aesthetic color.[5] Sky blue color of $SrCuSi_4O_{10}$ was modified into dark blue by doping the Eu^{3+} ion into Sr^{2+} and the NIR reflectance of the fabricated materials increased significantly by the substitution of 20% dopant in the host system.[6] $(Y_{1-x}R_x)_2Cu_2O_5$ (R = Gd^{3+}, Sc^{3+}, Yb^{3+} Lu^{3+} and Tm^{3+}) green pigments[7] were synthesized by the solid state reaction method and proved to be environmentally benevolent pigments compared to toxic Cr and Co green pigments. Pale yellow-colored $Y_6Mo_6O_{12}$ [Reflectance (R^*) = 92%] is converted into dark yellow-colored $Si_xY_{6-x}Mo_6O_{12}$ with R^* = 98% and dark brown color $Pr_xY_{6-x}Mo_6O_{12}$ with R^* = 60%.[8] Fe^{3+}-substituted $La_2Mo_2O_9$ nanocrystalline material with brilliant yellow color was developed with 92% reflectance, using the poly acryl amide method.[9] Red $Li_3InB_2O_6$[10] was prepared using the solid-state reaction method to obstruct the infrared radiations. The incorporation of V^{5+} ($3d^0$) in the pentavalent or the tetravalent site has been a promising strategy in recent years to obtain a yellow hue from white materials. In particular, vanadium in the pentavalent state (V_2O_5) is yellow due to the charge transfer transition from O_{2p} (II) to V_{3d} (V).[11] V-ZrO_2 is a well-known inorganic yellow pigment prepared by various conventional and non-conven-

Received: September 5, 2022
Accepted: November 17, 2022
Published: November 28, 2022

tional methods, evidencing the incorporation of V into ZrO_2 that induces the yellow hue in the resultant pigment material.[12] Gopal et al. reported the abnormal perception in the optical property of V^{5+}-substituted BPO_4. Open framework BPO_4 (white) was converted into yellow phosphovanadate by substituting the VO_4 site into the PO_4 site.[13] $BiVO_4$ was also proved as a promising yellow pigment in the industrial sector. Compiling all the preceding results, substitution or doping of bismuth and vanadium ions could be one of the iconic ideas to develop eco-friendly yellow pigments.

Lanthanide-based orthophosphates ($LnPO_4$) are recently materialized as an important class of inorganic substances, whose applications are widespread in various fields such as laser host materials, luminescent and phosphor materials, upconversion of photons, and bio-imaging.[14] These unique phosphates exhibit a variety of polymorphic forms, namely, monoclinic monazite, tetragonal xenotime, tetragonal zircon, monoclinic churchite, and hexagonal rhabdophane.[15] The formation of the foregoing crystal structures are decided by the synthesis methodology and the nature of the metal cation.[16] Some of the important rare earth phosphates that fit into the abovementioned profile are $CePO_4$, $PrPO_4$, YPO_4, $LuPO_4$, $LaPO_4$, $GaPO_4$, and $EuPO_4$. The physical, chemical, and optical properties of these materials were engineered by introducing a suitable substituent in the host lattice; hence the desired properties were achieved. Among various rare earth phosphates, yttrium phosphate (YPO_4) has versatile applications due to its sturdy nature and high chemical stability.[17] It exists in two distinctive crystal structures, namely, hexagonal (D_2 symmetry) and tetragonal (D_{2d} symmetry).[18] The tetragonal YPO_4 coexists with other elements in the mineral called xenotime,[19] which belongs to the space group of $I4_1/amd$, wherein the Y^{3+} ion follows D_{2d} symmetry. The structure of YPO_4 is formed by chains of corner-shared dodecahedron YO_8 and tetrahedron PO_4.[20]

YPO_4 is considered as one of the best host material to prepare luminescent compounds, since they acquire high quantum efficiency and because of the existence of explicit absorption and emission spectral regions.[21] High absorption and high vacuum stability during the radiation process in the ultraviolet (UV) domain make them as an efficient source of red light in normal and plasma display process.[22] Eu^{3+}-doped YPO_4 was reported to have the aforementioned quality; hence the possibility of using the material as a red light-emissive source was proposed by Chanchan and Singh.[21] Due to its high thermal expansion coefficient, it was explored as green barrier coatings to protect silicon ceramics. Ce^{3+} and Tb^{3+} co-doped yttrium phosphate was reported as potent glass ceramic material for WLED application due its adorable luminescent property on doping of a rare earth cation into yttrium lattice.[23] Dy^{3+}/YPO_4 and Sm^{3+}:YPO_4 co-doped with Bi^{3+} was reported as luminescent material with better emission intensity.[24,25]

As it is widely accepted that the optical, magnetic, and other physical/chemical properties are greatly influenced by the preparation methodology, it is necessary to carry out a detailed research so as to select a suitable method of synthesis to achieve the desired properties (exclusive size, shape, particle distribution, and crystallinity) on the resultant material.[26] Water-borne methods are much preferred over organic solvent-based methods due their non-toxic nature. A lot of research is being undertaken to synthesize micro- and nano-structured YPO_4 with desired properties, from the traditional solid state reaction route to versatile wet chemical routes, including precipitation method, hydrothermal method, solvo-thermal methods, and ion-exchange reactions.[27,28] Among these methods, the chemical co-precipitation method has attracted much attention due to high production and purity of the desired product, use of less or no organic solvents, good reproducibility of the product, and low production cost. In a typical precipitation method, expected products are precipitated as their hydroxides using appropriate precipitating agents such as ammonium hydroxide, NaOH, and tetra methyl ammonium hydroxide from the metal precursors, following the calcination process. Hence, in the current research, the precipitation method is preferred.[29]

Though YPO_4-based materials are studied for their luminescent property, it was not explored as a NIR-reflective pigment. To prove its application in another interesting field, herein, we investigated the NIR-reflective properties and color properties of YPO_4-, bismuth-, and vanadium-substituted YPO_4 synthesized by a simple precipitation method and demonstrated its excellence in cool coating applications.

2. MATERIALS AND METHODS

2.1. Materials. Yttrium oxide (99%), di-ammonium hydrogen phosphate (98%), aqueous ammonia (NH_4OH), bismuth nitrate penta hydrate (99%), and ammonium meta vanadate (98%) are used for the synthesis. All the chemicals were purchased from S.D. Fine Chemicals Private Limited, India, and used without further purification.

2.2. Method of Synthesis. $YP_{(1-x)}V_xO_4$ (x = 0, 0.05, 0.1, 0.15, 0.2, and 0.4), $Y_{(1-y)}Bi_yPO_4$ (y = 0.1 and 0.3), and $Y_{(1-x)}Bi_xP_{(1-y)}V_yO_4$ ($x = y$ = 0.2, 0.4, and 0.6) were prepared following the precipitation method. Details of the prepared samples and the corresponding sample are given in Table 1. To

Table 1. Prepared Samples and Its Acronyms

acronym	composition
YP	YPO_4
YV05	$YP_{0.95}V_{0.05}O_4$
YV1	$YP_{0.90}V_{0.10}O_4$
YV15	$YP_{0.85}V_{0.15}O_4$
YV2	$YP_{0.8}V_{0.2}O_4$
YV4	$YP_{0.6}V_{0.4}O_4$
YB1	$Y_{0.9}Bi_{0.1}PO_4$
YB3	$Y_{0.7}Bi_{0.3}PO_4$
YB2V2	$Y_{0.9}Bi_{0.2}P_{0.8}V_{0.2}O_4$
YB4V4	$Y_{0.6}Bi_{0.4}P_{0.6}V_{0.4}O_4$
YB6V6	$Y_{0.4}Bi_{0.6}P_{0.4}V_{0.6}O_4$

synthesize yttrium phosphate, 1 M of yttrium oxide was dissolved 1:1 HNO_3. To this, 1 M of di-ammonium hydrogen phosphate was added drop by drop, after which the pH of the resulting solution was adjusted to 4. Once the precipitation is completed, it was washed with distilled water, filtered, and dried in an oven at 100 °C. The dried precursor powder was ground well and subjected to calcinations at 300, 500, and 900 °C. To synthesize bismuth-substituted yttrium phosphate, bismuth nitrate solution was added along with yttrium nitrate solution and the abovementioned process was repeated. To synthesize vanadium-substituted materials, yellow ammonium meta vanadate solution which was pre-dissolved using 1:1 HNO_3 was added after adding ammonium phosphate solution.

2.3. Chemical Stability Test and Thermal Stability Test. Concerning the stability of the pigment toward

https://doi.org/10.1021/acsomega.2c05748
ACS Omega 2022, 7, 44266−44277

aggressive chemicals, 100 mg of specific pigment was soaked in 2% HNO_3, 2% H_2SO_4, 2% NaOH, and 2% HCl individually and stirred for an hour. Treated pigments were strained using filter paper, rinsed using distilled water, and air dried, and their weight was re-examined. Thermal stability of the particular pigment was studied by subjecting it to high calcination temperatures from 900 to 1100 °C for 6 h.

2.4. Characterization Techniques. The powder X-ray diffraction (PXRD) technique was employed to identify the phase formation of synthesized materials. Structural analysis was accomplished using the BRUKER D8 Advanced instrument via a Cu K alpha radiation with 1.54056 Å handling wavelength. The lattice parameter of the synthesized materials was calculated using powder X software. AlO_4, PO_4, and Al−O stretching and bending vibrations and the functional groups present in the fabricated pigment components were recognized with the Fourier transform infrared spectroscopy (FT-IR) technique in the 400 and 4000 cm^{-1} range with the JASCO FT-IR instrument. The modification in the morphology due to substitution and the presence of elements were established using the ZESIS EVO18 scanning electron microscopy (SEM) instrument. HR-TEM (FEI-TECHNAI, G2-20 TWIN) with the operating voltage of 200 kV was employed to analyze the detailed morphology of the selected pigment particle, and the selected area diffraction pattern (SAED) was also employed with the same instrument. Absorbance and diffuse reflectance spectra were recorded using the JASCO-V670 UV-DRS spectrophotometer in the 200 to 2500 nm operating range with the step size of 1 nm. The color coordinates such as L^* = lightness or darkness of the pigment (0−100), a^* value representing the greenness ($-a^*$) or redness ($+a^*$), and b^* values representing the yellowness ($+b^*$) and blueness ($-b^*$) of any synthesized material were calculated according to the recommendation by Commission Internationale de l'Eclairage (CIE) using D 65 illuminant through a 10° viewer angle. The amount of saturation is calculated with the term Chroma (C), which can be calculated by $C = \sqrt{a^{*2} + b^{*2}}$. The hue in the cylindrical color space extends from 0 to 360°, which could be found by the formula (h^o =$\tan^{-1}$ (b^*|a^*). NIR reflectance (R^*) of the fabricated materials was found via the following formula

$$R^* = \frac{\int_{700}^{2500} r(\lambda)\cdot i(\lambda)\cdot d(\lambda)}{\int_{700}^{2500} i(\lambda)\cdot d(\lambda)}$$

At this juncture, the reflectance acquired from the experimental data is noted as $r(\lambda)$ and the solar irradiance is termed as $i(\lambda)$ with the unit of (W/m^2·nm).

3. RESULTS AND DISCUSSION

3.1. TGA/DTA Analysis. Simultaneous TGA/DTA was carried out to identify the thermal properties of YPO_4. Two stages of weight losses were observed from thermogravimetric analysis, as shown in Figure 1. According to Figure 1, a total weight loss of 11.5% was observed after thermal treatment from ambient temperature to 1200 °C. Initial weight loss of about 8.7% was noticed from 100 to 400 °C, and further increase in temperature till 800 °C brought a slight weight loss of around 2.8%,[30] after which no significant weight loss was observed, which showed that the system is stable above 800 °C due to the loss of lattice water. The DTA curve showed an endothermic peak below 100 °C, which was attributed to the disappearance of water molecules and nitrates.

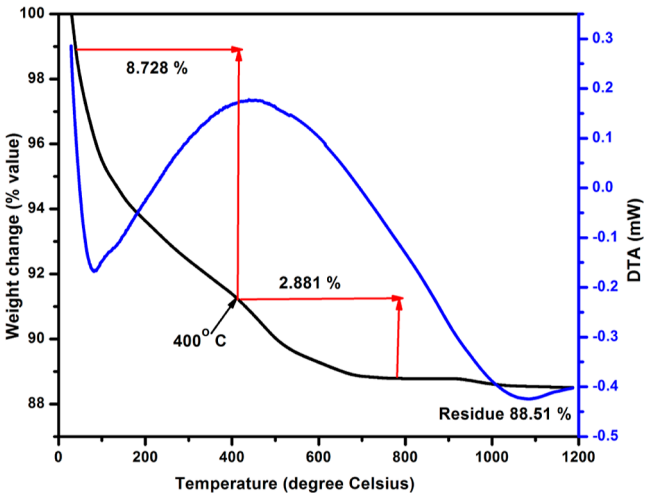

Figure 1. TGA/DTA analysis of YPO_4.

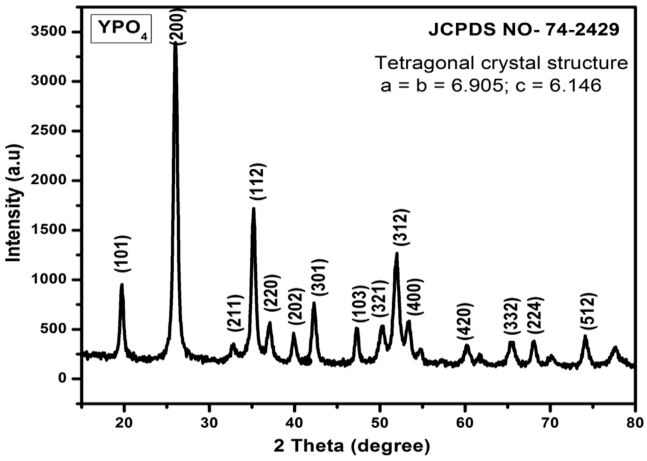

Figure 2. PXRD pattern of YPO_4.

3.2. PXRD Analysis. The PXRD technique was employed to identify the crystal structure, phase purity, lattice details, and the average crystallite size of the synthesized materials. Figure 2 shows the PXRD pattern of YPO_4. Peaks corresponding to 2θ angle observed are well harmonized with the standard structure (JCPDS. no. 74-2429) with the space group of $I4_1/amd$,[31] and the lattice values are found to be $a = b = 6.913$, $c = 6.174$ with the average crystallite size of 34 nm. Table 1 shows the prepared pigments and its acronyms.

3.2.1. Effect of Vanadium Substitution on the Structure of YPO_4. Figure 3a shows the diffraction pattern of $YP_{1-x}V_xO_4$, x = 0.05, 0.1, 0.15, and 0.2 prepared by the chemical precipitation method. One could affirm the formation of the tetragonal structure after the substitution of V^{5+} into P^{5+} lattice with the shift in the diffraction peak to lower theta angle (Figure 3b). The shift is obvious due to the substitution of higher ionic radii (0.36 Å) V^{5+} with lower ionic radii (0.17 Å) P^{5+} having the co-ordination number of 4. Due to this substitution, lattice strain in the crystal structure occurs owing to inadequate ionic radii of P^{5+}, which could not accommodate bigger V^{5+} in its lattice and possibly shifted the high intense peak in the direction of the lower theta angle.[32] Further addition of V^{5+} (x = 0.4) leads to the formation of secondary

https://doi.org/10.1021/acsomega.2c05748
ACS Omega 2022, 7, 44266−44277

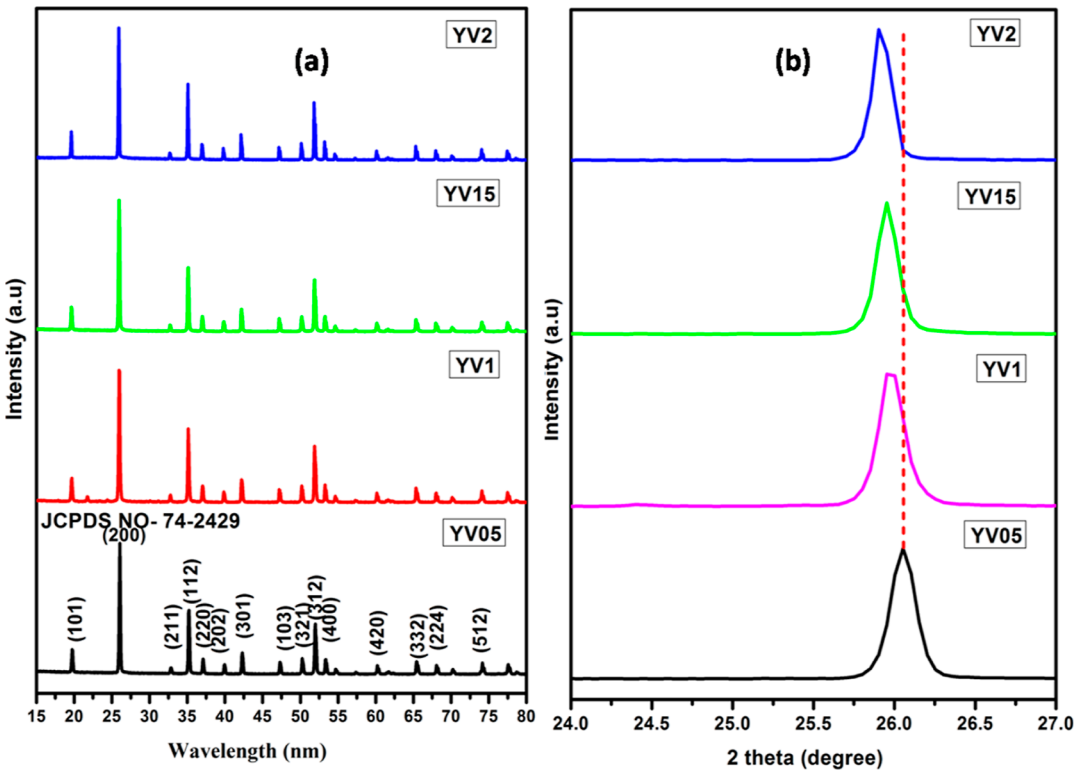

Figure 3. (a) $YP_{1-x}V_xO_4$, x = 0.05, 0.1, 0.15, and 0.2. (b) Expanded view.

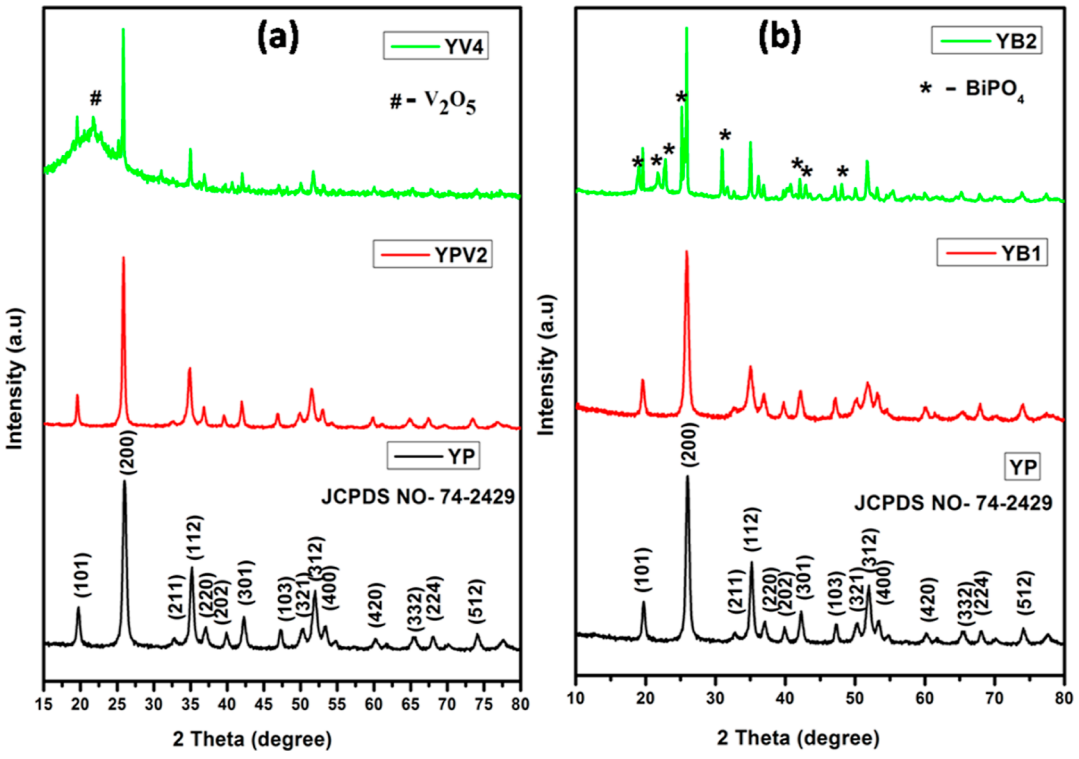

Figure 4. PXRD pattern of (a) $YP_{1-x}V_xO_4$ (x = 0, 0.2, and 0.4). (b) $Y_{1-x}Bi_xPO_4$ (x = 0, 0.1, and 0.2).

phase V_2O_5 in the YPO_4 structure (Figure 4a). Comparable finding was discerned by Wujczyk et al.[20] In the above-mentioned research, a series of luminescent materials were formed by doping Er^{3+} and Tm^{3+} co-doped with Yb^{3+} in $YP_{1-x}V_xO_4$ (x = 0−1.0). They concluded that lattice strain and shift in diffraction peaks toward the lower angle is due to V^{5+} replacement and not due to the other rare earth ions present.

3.2.2. Effect of Bismuth Substitution on the Structure of YPO_4. Figure 4b depicts the PXRD spectra of $Y_{1-y}Bi_yPO_4$ (y = 0, 0.1, and 0.2). When y = 0.1, that is, $Y_{0.9}Bi_{0.1}PO_4$, we could observe the formation of the tetragonal crystal structure

https://doi.org/10.1021/acsomega.2c05748
ACS Omega 2022, 7, 44266−44277

Table 2. 2 Theta and R.P.I Values of $YP_{1-x}V_xO_4$, x = 0, 0.05, 0.1, 0.15, and 0.2) and $Y_{0.9}Bi_{0.1}PO_4$

YP		YV05		YV1		YV15		YV2		YB1	
2θ	[a]R.P.I	2θ	[a]R.P.I	2θ	[a]R.P.I	2θ	[a]R.P.I	2θ	[a]R.P.I	2θ	[a]R.P.I
19.751	973	19.723	969	19.719	978	19.711	945	19.698	986	19.715	792
25.932	3465	25.927	2920	25.910	2858	25.865	2789	25.804	2788	25.807	2756
32.633	385	32.629	450	32.620	378	32.608	365	32.596	340	32.760	333
35.275	1757	35.268	1749	35.256	1787	35.289	1723	35.265	1748	35.065	984
37.138	583	37.136	580	37.128	575	37.121	563	37.117	598	36.913	612
39.867	488	39.765	476	39.667	497	39.546	465	39.446	472	39.804	447
42.323	790	42.312	795	42.309	778	42.324	765	42.319	758	42.237	588
47.103	537	47.97	528	47.94	549	47.925	556	47.893	543	47.086	497
50.294	530	50.281	514	50.276	528	50.286	535	50.283	546	50.178	497
51.911	1291	51.891	1285	51.880	1274	51.876	1269	51.860	1245	51.845	734
53.385	576	53.378	586	53.369	592	53.360	567	53.367	583	53.365	576
60.348	375	60.343	363	60.339	397	60.326	384	60.321	384	59.923	340
65.544	392	65.539	373	65.520	365	65.513	386	65.497	395	65.512	269
67.999	392	67.986	385	67.964	374	67.986	358	67.976	376	67.839	400
74.281	441	74.276	435	74.276	467	74.275	456	74.263	472	74.042	400

[a]Relative peak intensity.

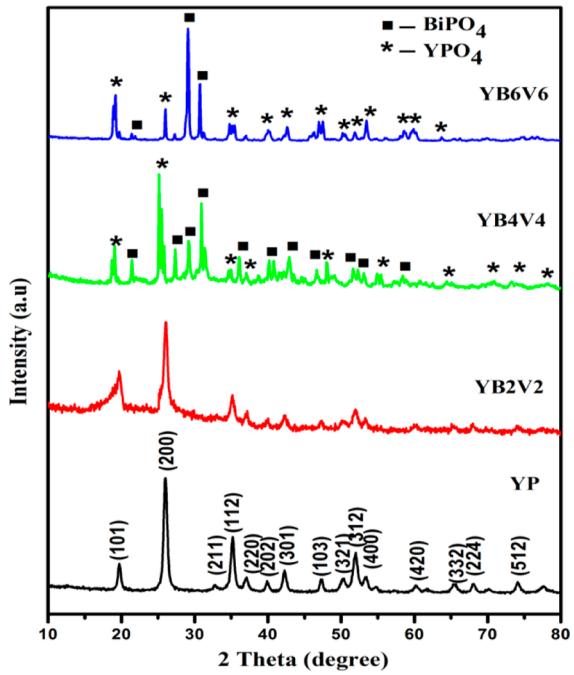

Figure 5. PXRD pattern of $Y_{1-x}Bi_xP_{1-y}V_yO_4$ ($x = y$ = 0, 0.2, 0.4, and 0.6).

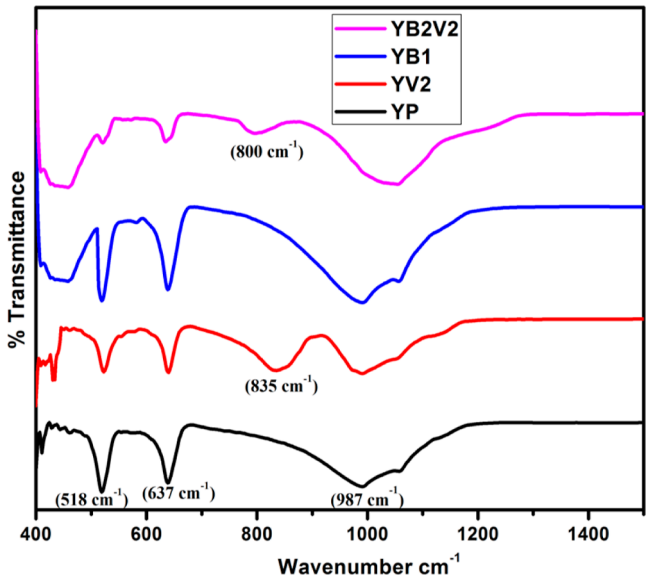

Figure 6. FT-IR spectra of YPO_4, $YP_{0.8}V_{0.2}O_4$, $Y_{0.9}Bi_{0.1}PO_4$, $Y_{0.8}Bi_{0.2}P_{0.8}V_{0.2}O_4$.

without the formation of secondary phase. However, at y = 0.2, $Y_{0.8}Bi_{0.2}O_4$, bismuth phosphate as $BiPO_4$ appeared as a secondary phase. Emergence of the secondary phase was noticed due to the substitution of larger Bi^{3+} (ionic radii of bismuth = 1.03 Å) into smaller Y^{3+} (ionic radii of yttrium = 0.9 Å) lattice, which leads to lattice expansion.[33] Higher loading of bismuth ion resulted in concoction of YPO_4 and $BiPO_4$ phases. Lower and higher substitution of bismuth into YPO_4 lattice did not result in the expected color; therefore, synthesis of this series was not continued. Table 2 shows 2 theta and relative peak intensity (R.P.I) values of $YP_{1-x}V_xO_4$, x = 0, 0.05, 0.1, 0.15, and 0.2) and $Y_{0.9}Bi_{0.1}PO_4$.

3.2.3. Effect of Simultaneous Substitution of Both V^{5+} and Bi^{3+} into YPO_4 Lattice. Figure 5 shows the PXRD spectra of $Y_{1-x}Bi_xP_{1-y}V_yO_4$ ($x = y$ = 0, 0.2, 0.4, and 0.6). Co-substitution of bismuth and vanadium in the YPO_4 lattice was proposed to improve its color properties. At $x = y$ = 0.2, one could not notice any secondary phase formation. Higher substitution leads to the formation of mixed phases of YPO_4 and $BiPO_4$. Absence of V_2O_5 as the secondary phase is due to the possibility of iso-structural formation of YPO_4 and YVO_4.[29]

3.3. Investigation on the FT-IR and Raman Spectra of Synthesized Materials. The interaction between the metal ions present (Y, V, P, Bi, and O) in the fabricated materials with oxide ion (O^{2-}) is identified by decoding the FT-IR spectra of the materials YPO_4, $YP_{0.8}V_{0.2}O_4$, $Y_{0.9}Bi_{0.1}PO_4$, and $Y_{0.8}Bi_{0.2}P_{0.8}V_{0.2}O_4$, as illustrated in Figure 6. In all the portrayed samples, two different significant vibrations were noticed at 637 and 518 cm^{-1} corresponding to $(PO_4)^{3-}$ phosphate moiety, due to distorted cockeyed vibrations. A peak at 987 cm^{-1} is due to P−O stretching vibrations.[34−36] An additional vibration at 835 and 800 cm^{-1} was noticed for YV2 and YB2V2 due to the presence of VO_4^{3-}. A similar observation was noticed when Eu^{3+} and V^{5+} were doped into YPO_4 lattice.[34]

https://doi.org/10.1021/acsomega.2c05748
ACS Omega 2022, 7, 44266−44277

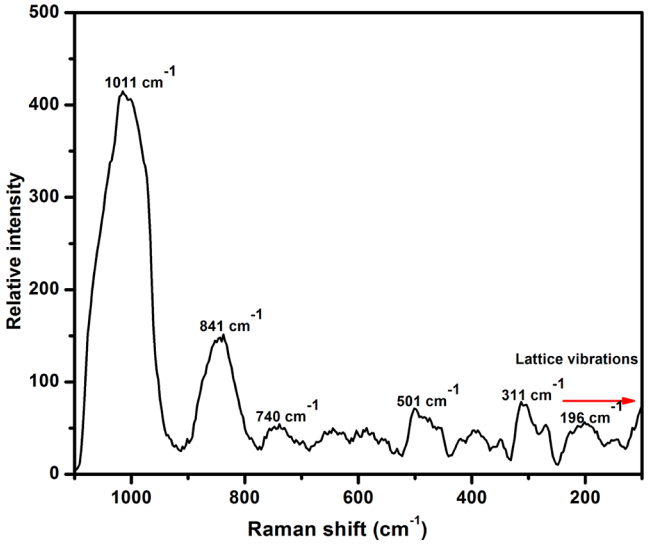

Figure 7. Raman spectrum of $Y_{0.8}Bi_{0.2}P_{0.8}V_{0.2}O_4$.

The presence of metal oxide vibrations such as Bi−O and Y−O is noticed between 400 and 450 cm^{-1}.[37] The abovementioned results emphasized the formation of yttrium phosphate-, vanadium-, and bismuth-doped yttrium phosphates.

Raman spectral analysis of $Y_{0.8}Bi_{0.2}P_{0.8}V_{0.2}O_4$ was carried out to identify the necessary vibration in the material, and the spectrum is depicted in Figure 7. As shown in Figure 7, the spectrum consists of various Raman vibrations that correspond to VO_4, PO_4, and Bi−O vibrations. The Raman shifts observed at 1011 cm^{-1} refer to asymmetric stretching vibrations of the PO_4 group. The peaks at 501 cm^{-1} corresponding to bending mode of the PO_4 group and the band at 196 cm^{-1} could be due to O−Bi−O bending mode of vibrations.[38,39] VO_4 stretching vibrations are observed at 841 cm^{-1}.[40] Significant vibrations indicate the presence of metal oxide bonding, phosphate, and vanadate moiety in the YB2V2 material.

3.4. X-ray Photoelectron Spectroscopy Analysis. To appreciate the chemical state of all the metal cations present in the prepared sample, XPS was carried out. Figure 8 depicts the XPS spectra of $Y_{0.4}Bi_{0.6}P_{0.4}V_{0.6}O_4$ (as a representation) synthesized by the chemical precipitation method. Standard C 1s binding energy was compared with C 1s energy obtained by the experiment, and the results are used to calibrate of binding energy of elements present in the system. The high resolution peak are fitted to show Y 3d, P 2p, V 2p, O 1s, and Bi 4f states present in the material. The valence energy state of metal ions is identified based on their binding energy locations. The Y 3d state was recognized by the presence of peaks at 157.17 and 158.88 eV corresponding to $3d_{5/2}$ and $3d_{3/2}$.[41] Phosphorous in its +5 oxidation state was identified by the

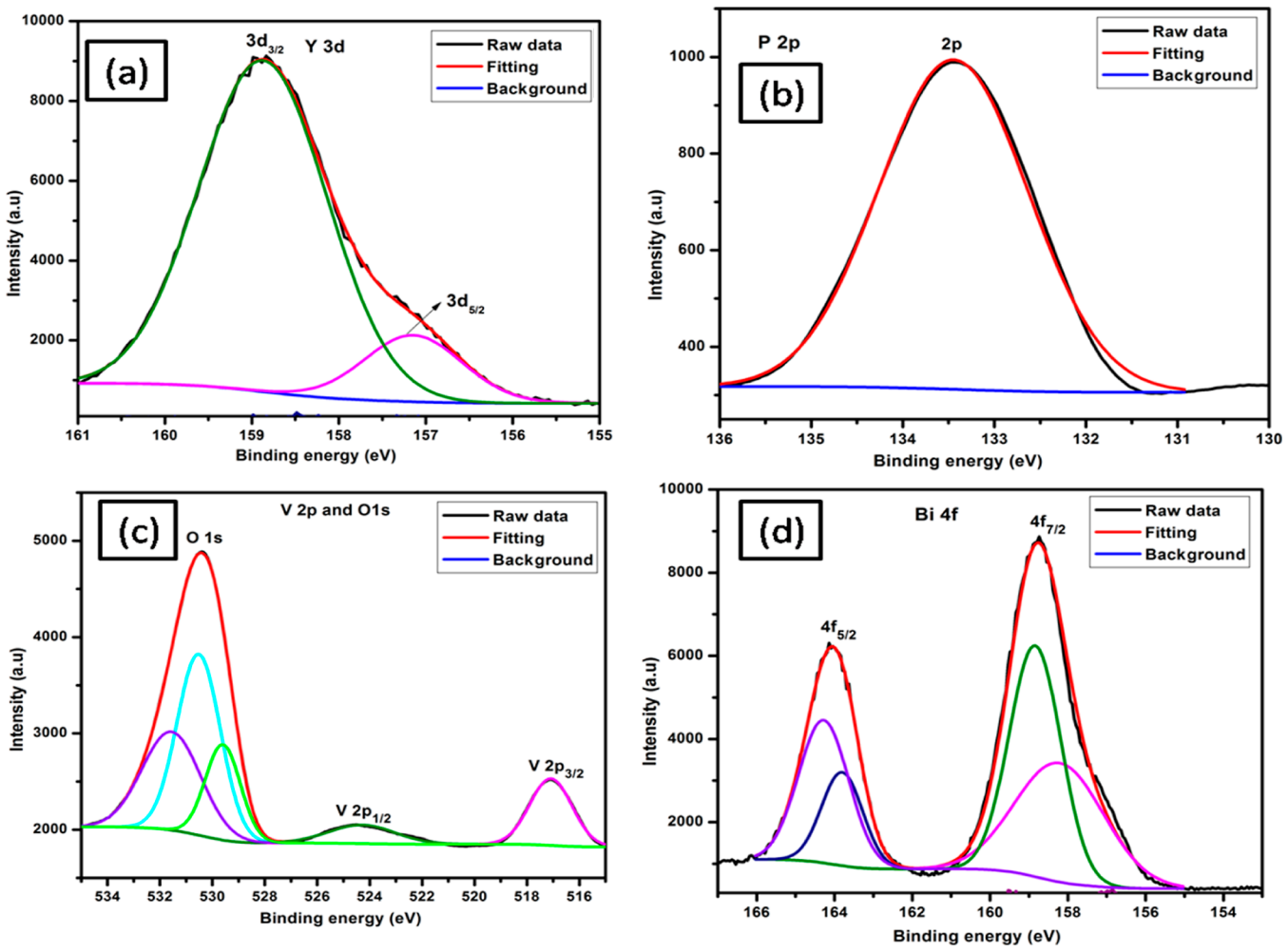

Figure 8. XPS spectra of $Y_{0.4}Bi_{0.6}P_{0.4}V_{0.6}O_4$. (a) Y 3d, (b) P 2p, (c) V 2p and O 1s, (d) Bi 4f.

https://doi.org/10.1021/acsomega.2c05748
ACS Omega 2022, 7, 44266−44277

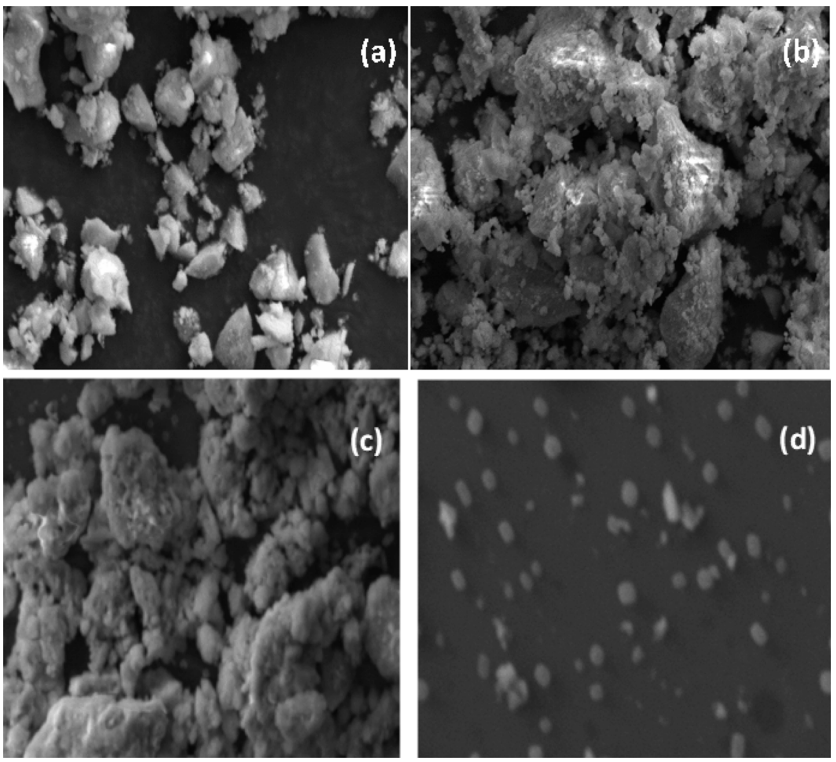

Figure 9. SEM images of (a) YPO_4, (b) $YP_{0.8}V_{0.2}O_4$, (c) $Y_{0.9}Bi_{0.1}PO_4$, and (d) $Y_{0.4}Bi_{0.6}P_{0.4}V_{0.6}O_4$ pigments.

Table 3. Elemental Composition of the Selected Materials Obtained from EDAX Analysis

composition	element	weight %	atomic %
$Y_{0.9}Bi_{0.1}PO_4$	Y	17.23	3.53
	Bi	3.81	0.33
	P	3.13	1.84
	O	83.44	94.96
	total	100	
$Y_{0.4}Bi_{0.6}P_{0.4}V_{0.6}O_4$	Y	14.28	3.47
	P	1.58	1.10
	Bi	12.14	1.26
	V	3.40	1.44
	O	68.60	92.73
	total	100	

existence of a peak at 133.32 eV, suggesting the presence of the P 2p energy level of the cation. From the figure, one could confirm the presence of the V 2p state by observing the binding energy at 517 eV corresponding to the V $2p_{1/2}$ level and 524.53 eV corresponding to the V $2p_{3/2}$ level. Parhi and Manivannan[42] reported the existence of the V $2p_{1/2}$ energy level at 518.4 eV in YVO_4. A shift in the peak position to a lower energy level is noticed in the current investigation, which could be due to the substitution effect. The deconvoluted spectrum of oxygen also presented in the same illustration. Here, the O 1s core level is fitted by the presence of three binding energies centered at 531.64, 530.57, and 529.61 eV corresponding to the surface hydroxyl group, oxygen in the surface lattice, and the metal−oxygen bond present in the material.[43] Significant spin orbit doublets, namely, Bi $4f_{5/2}$ and Bi $4f_{7/2}$ were centered at 158.71 and 164.12 eV, which confirmed the presence of bismuth in its +3 oxidation state. These doublet peaks are further deconvoluted, resulting in four different binding energies found at 158.81, 158.29, 163.76, and 164.29 eV.[44]

3.5. SEM, TEM, and EDAX Analyses. SEM micrographs of YPO_4, $YP_{0.8}V_{0.2}O_4$, $Y_{0.9}Bi_{0.1}PO_4$, and $Y_{0.4}Bi_{0.6}P_{0.4}V_{0.6}O_4$ are illustrated in Figure 9. The images clearly show that the particles are highly aggregated due to the rapid growth of particles during the precipitation reaction. This process of aggregation of nanoparticles begins at the stage of pre-nuclei formation after the dissolution of precursor materials. The nanoparticles are formed after the formation of a new boundary between the nuclei due to the free energy supplied to them. However, in some cases, there is a possibility of formation of pre-nucleation clusters, which leads to aggregation of small particles. Such aggregated particles are very stable and difficult to separate during mechanical grinding.[45] No significant change in the morphology was identified due to the introduction of vanadium and bismuth into tetragonal YPO_4, whereas co-substitution of both vanadium and bismuth in the YPO_4 lattice induced the change in morphology as a well-defined rectangular particle, which is clearly seen in Figure 9. The change in morphology could be due to the substitution effect.[46] The elemental composition obtained from EDAX analysis of selected elements is tabulated in Table 3, which confirmed the presence of Y, P, V, Al, Bi, and O in the currently reported materials. In order to arrive at a better conclusion about the morphology of the fabricated materials, TEM analysis was carried out. Figure 10 shows the TEM and EDAX images of $Y_{0.4}Bi_{0.6}P_{0.4}V_{0.6}O_4$. Rectangular-shaped particles with particle size ranging between 85 and 100 nm are obtained, which are in good agreement with the results obtained by PXRD. Dark spots from the SAED pattern indicates the crystalline nature of the sample.

3.6. UV-DRS Analysis. Figure 11 shows the UV-DRS spectra of YPO_4, $YP_{1-x}V_xO_4$ (x = 0.05, 0.1, 0.15, 0.2, and 0.4),

https://doi.org/10.1021/acsomega.2c05748
ACS Omega 2022, 7, 44266−44277

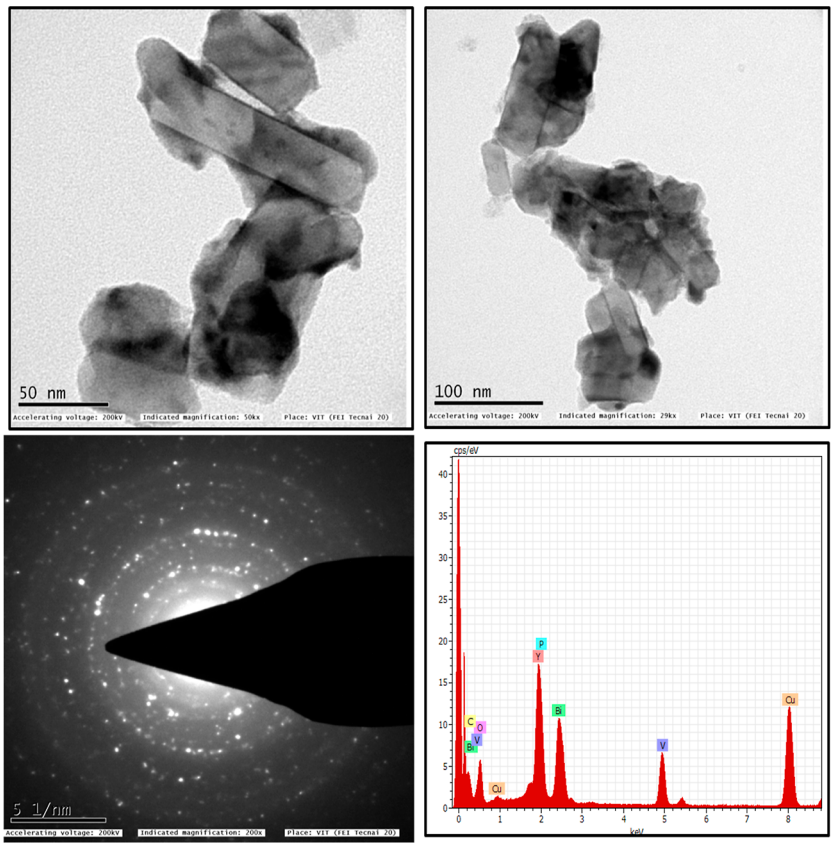

Figure 10. TEM images and EDAX spectrum of the $Y_{0.4}Bi_{0.6}P_{0.4}V_{0.6}O_4$ pigment.

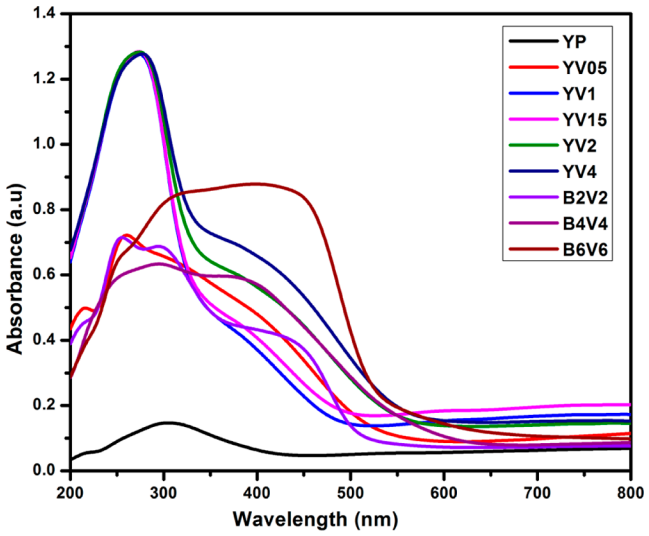

Figure 11. UV-DRS spectrum of YPO_4, $YP_{1-x}V_xO_4$ (x = 0.05, 0.1, 0.15, 0.2, and 0.4), and $Y_{1-x}Bi_xP_{1-y}V_yO_4$ ($x = y$ = 0, 0.2, 0.4, and 0.6).

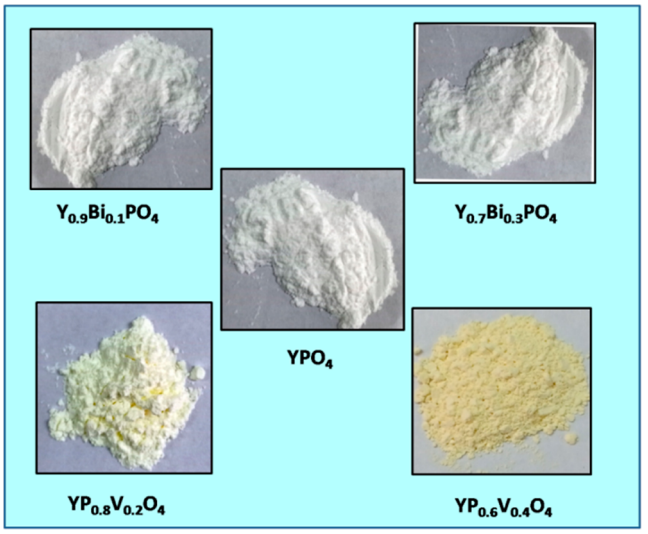

Figure 12. Digital images of YPO_4, $YP_{1-x}V_xO_4$ (x = 0.2 and 0.4), and $Y_{1-x}Bi_xPO_4$ (x = 0.1, and 0.3).

and $Y_{1-x}Bi_xP_{1-y}V_yO_4$ ($x = y$ = 0, 0.2, 0.4, and 0.6) prepared using the precipitation method. As mentioned in another study, YPO_4 shows a weak absorption peak between 230 and 330 nm due to charge transfer transition between the divalent oxygen anion (O_2^{2-}) and the pentavalent phosphorus cation (P^{5+}),[47] and the color of material was found to be white. An additional transition between 350 and 470 nm was perceived because of the increase in vanadium content and due to the charge transfer between $V^{5+}-O^{2-}$ rather than d−d transition, since V^{5+} had a d^0 electronic configuration.[48] As a result, yellow tinge was developed for the engineered materials. Bismuth and vanadium co-substituted materials slowly shifted the absorption maximum to higher wavelength, and it reached to 450 nm while substituting 60% of bismuth and vanadium in the YPO_4 lattice. Since 400−450 nm is a violet region, its complementary yellow color is observed. Here, introduction of vanadium in the phosphorous lattice produces VO_4^{3-} transition. Along with this VO_4^{3-} transition, a hybrid orbital transition is also possible from the mixture of Bi 6s and O 2p orbitals to V 3d orbitals.[49] The abovementioned phenomenon

https://doi.org/10.1021/acsomega.2c05748
ACS Omega 2022, 7, 44266−44277

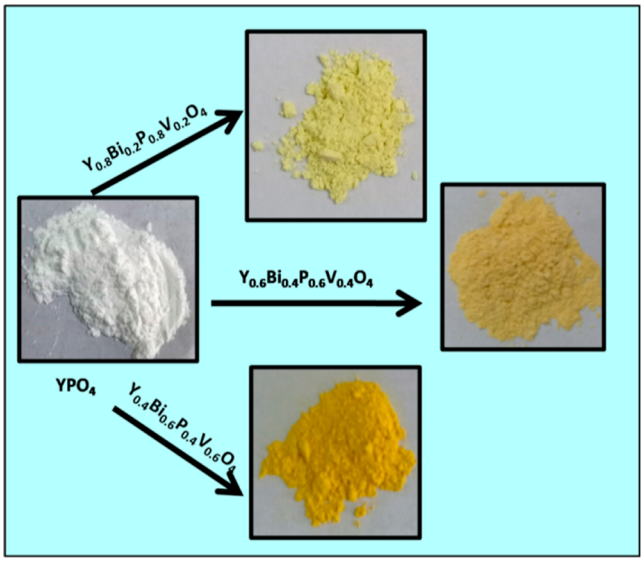

Figure 13. Digital images of $Y_{1-x}Bi_xP_{1-y}V_yO_4$ ($x = y = 0$, 0.2, 0.4, and 0.6).

is responsible for the intense yellow color of the co-doped materials.

The digital images of vanadium-substituted YPO_4 and bismuth and vanadium co-substituted YPO_4 are presented in Figures 12 and 13, respectively, and their corresponding color values are tabulated in Table 4. When $x = 0$, a negative b^* (−1.29) value was obtained, confirming their white color. Substitution of bismuth into yttrium lattice does not significantly affect the color; hence they are white, which is further confirmed by its corresponding color values. Substitution of 0.2 M of vanadium slightly increased the yellow tinge of material to +15.71. 0.4 M of vanadium in the P^{5+} increased the yellowness of the material to +26.6 with a slight decrease in lightness of the material. Here, the amount of V^{5+} content was doubled from 0.2 to 0.4 M so as to increase the yellow hue of the pigment. Further addition of V^{5+} in the YPO_4 structure did not increase the b^* value. Simultaneous addition of both bismuth and vanadium in the YPO_4 steadily increased the yellowness value from +26.16 to +56.06 (Table 4). The hue angle represents the color of the system in terms of angular position in the cylindrical color space. It is observed from the literature, if the hue angle was found to be between 70 and 105°, the material will exhibit yellow color. All the optically engineered materials in the current study are having the hue angle between 70 and 90°, which confirmed the yellow color of the pigments.

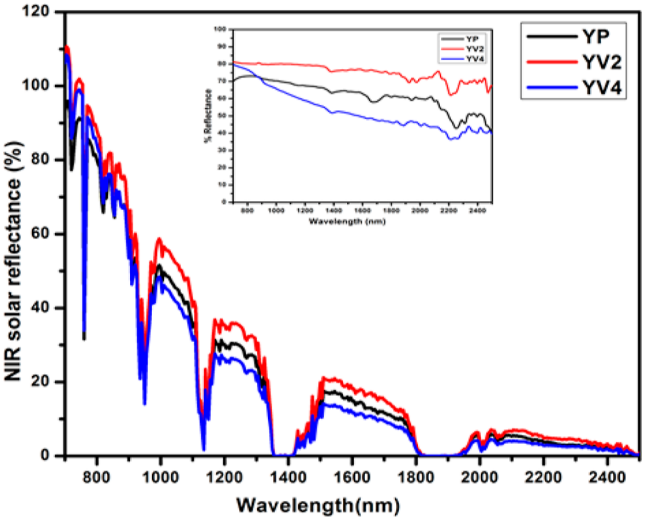

Figure 14. NIR solar reflectance spectrum of $YP_{1-x}V_xO_4$ ($x = 0$, 0.2, and 0.4); reflectance spectra are provided in the inset.

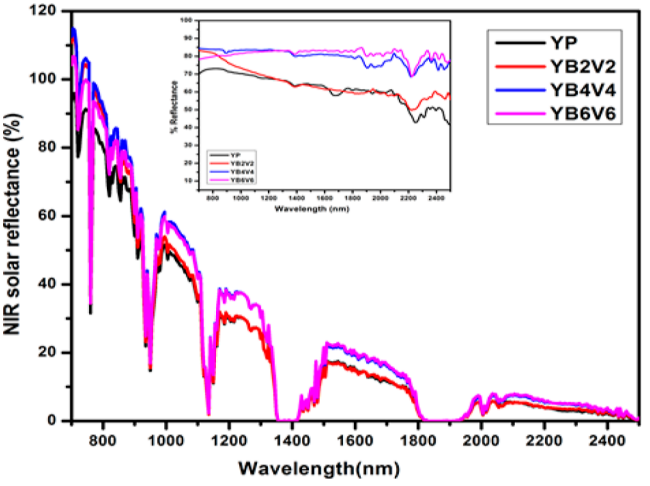

Figure 15. NIR solar reflectance spectrum of $Y_{1-x}Bi_xP_{1-y}V_yO_4$ ($x = y = 0$, 0.2, 0.4, and 0.6).

3.7. NIR Reflectance Analysis. Figures 14 and 15 show the NIR reflectance of $YP_{1-x}V_xO_4$ ($x = 0$, 0.2, and 0.4) and $Y_{1-x}Bi_xP_{1-y}V_yO_4$ ($x = y = 0$, 0.2, 0.4, and 0.6). The NIR solar reflectance of white YPO_4 in the 800−2500 nm NIR region was found to be 68%. Significant increase in the NIR reflectance was observed after the addition of 0.2 M of V^{5+} ion in the YPO_4 structure. Nearly 10% increase in the reflectance was noticed; hence, the NIR reflectance increased

Table 4. Color Properties and NIR Solar Reflectance of Synthesized Compounds

	color co-ordinates					
compounds	L	a^*	b^*	C^*	$h°$	NIR solar reflectance R^* (%)
YPO_4	95.09	0.56	−1.29	1.41	26.53	68
$Y_{0.9}Bi_{0.1}PO_4$	96.23	2.00	1.26	1.72	32.21	81
$Y_{0.7}Bi_{0.3}PO_4$	94.78	1.78	1.90	1.89	46.86	65
$YP_{0.8}V_{0.2}O_4$	95.97	−1.02	5.71	5.23	77.96	78
$YP_{0.6}V_{0.4}O_4$	89.36	−2.86	25.62	26.16	87.48	64
$Y_{0.8}Bi_{0.2}P_{0.8}V_{0.2}O_4$	85	4.20	30.14	31.54	82.06	72
$Y_{0.6}Bi_{0.4}P_{0.6}V_{0.4}O_4$	91.35	−5.81	30.55	35.76	87.68	82
$Y_{0.4}Bi_{0.6}P_{0.4}V_{0.6}O_4$	81.36	1.87	56.06	60.25	88.08	83

https://doi.org/10.1021/acsomega.2c05748
ACS Omega 2022, 7, 44266−44277

Table 5. Color Values of $Y_{0.4}Bi_{0.6}P_{0.4}V_{0.6}O_4$ after Chemical and Thermal Treatment

	color parameters		
2% acid or alkali	L^*	a^*	b^*
	81.36	1.87	56.06
NaOH	82.40	1.73	55.93
HNO_3	83.98	1.69	54.82
HCl	81.28	1.85	55.92
H_2SO_4	81.40	1.89	56.04
	Thermal Stability		
900 °C	81.36	1.87	56.06
1000 °C	78.46	1.12	63.49
1200 °C	50.65	0.65	70.64

from 68 to 78%. Further addition of V^{5+}, that is, 0.4 M addition of vanadium content significantly reduced the NIR reflectance from 68 to 64%. Concurrent addition of both bismuth and vanadium in the YPO_4 structure increased the NIR reflectance of the hybrid material gradually and it reached to 82% for $Y_{0.4}Bi_{0.6}P_{0.4}V_{0.6}O_4$. The reason for the increase in reflectance of material is explained due to the morphology change that occurred during co-substitution of both bismuth and vanadium in the YPO_4 structure. According to the Kubelka–Munk (KM) theory, the mean particle size (d) is inversely related to the scattering coefficient (S). Hence, if the mean particle size is less (d < 1 μm), the scattering efficiency of the material increases, which in turn increases the reflectance.[50] In the current study, the co-substituted materials have the least mean particle size of 98 nm (YB6V6), 83 nm (YB4V4), 112 nm (YB2V2) compared to vanadium-substituted YPO_4 materials. According to KM theory, more regular particles with a definite morphology are also important for high NIR reflectance. Rectangular-shaped particles with more regular distribution could be one of the important reasons for high reflectance of YB6V6. The abovementioned result was supported by Tao et al., who stated that the high reflectance could be due to the uniformed spherical particles and low particle size.[51]

3.8. Chemical and Thermal Stability Test. Table 5 shows the CIE Lab color values of $Y_{0.4}Bi_{0.6}P_{0.4}V_{0.6}O_4$ after it was subjected to chemical and thermal treatment. From the results, one could observe very less change in the b^* value after treating with 2% acid and base medium and a negligible amount of weight loss, indicating that they are chemically stable and can be used as metallic coating materials. To check the suitability of the material for the application in ceramic and glaze substances, it was calcined to higher temperatures from 900 to 1000 °C and 1200 °C. As the temperature increases, we could observe that the b^* value increases from 56.06 to 70.64, which shows that the yellowness value increases as the temperature increases.

4. CONCLUSIONS

Tetragonal YPO_4-, vanadium-, and bismuth-substituted YPO_4 and Bi and V co-substituted YPO_4 are prepared by a simple precipitation method and authenticated by PXRD, FTIR, and Raman spectroscopy. From XRD, we could notice that 0.4 M of vanadium substitution into the YPO_4 structure formed a secondary phase structure V_2O_5, whereas the color of the material changed from white to yellow. Substitution of bismuth into the YPO_4 structure does not increase the b^* value, which proved that the bismuth ion does not play a significant role in the formation of yellow color of the pigment, while influence of vanadium in the development of yellow color is noticed. On the other hand, co-substitution of both vanadium and bismuth in the YPO_4 lattice enhanced the b^* value and NIR reflectance. $Y_{0.4}Bi_{0.6}P_{0.4}V_{0.6}O_4$ showed 83% NIR solar reflectance, and its b^* value was also found to be higher (56.06). The reason for higher reflectance could be due to the formation of more uniform particles, which was confirmed by TEM images. The fabricated material was found to be stable while treating with 2% H_2SO_4. Higher thermal treatments (subjected to calcination at 1000 and 1200 °C) increased the b^* value of YB6V6 to 63.49 and 70.64. Hence, with higher b^* and NIR solar reflectance, $Y_{0.4}Bi_{0.6}P_{0.4}V_{0.6}O$ could serve as an environmentally benign cool yellow pigment.

AUTHOR INFORMATION

Corresponding Author

Shanmugam Sumathi − *Department of Chemistry, School of Advanced Sciences, Vellore Institute of Technology, Vellore 632014, India;* orcid.org/0000-0003-1724-1719; Email: sumathishanmugam2003@gmail.com

Author

Vasudevan Elakkiya − *Department of Chemistry, School of Advanced Sciences, Vellore Institute of Technology, Vellore 632014, India*

Complete contact information is available at: https://pubs.acs.org/10.1021/acsomega.2c05748

Notes

The authors declare no competing financial interest.

ACKNOWLEDGMENTS

The authors acknowledge VIT, Vellore, for providing lab facility to perform research. S.S. and V.E. would like to acknowledge Council of Scientific and Industrial Research (CSIR), New Delhi, Government of India, for the financial support toward Extramural research fund [01(3085)21/EMR/-II] and Senior Research Fellowship [file no. 09/844/(0098)/2020-EMR-1].

REFERENCES

(1) Li, Q.; Zhang, H.; Liu, X.; Huang, J. Urban heat island effect on annual mean temperature during the last 50 years in China. *Theor. Appl. Climatol.* **2004**, *79*, 165−174.

(2) Chua, K. J.; Chou, S. K.; Yang, W. M.; Yan, J. Achieving better energy-efficient air conditioning - A review of technologies and strategies. *Appl. Energy* **2013**, *104*, 87−104.

(3) Bretz, S.; Akbari, H.; Rosenfeld, A. Practical issues for using solar-reflective materials to mitigate urban heat islands. *Atmos. Environ.* **1998**, *32*, 95−101.

(4) Pisello, A. L.; Cotana, F.; Brinchi, L. On a cool coating for roof clay tiles: development of the prototype and thermal-energy assessment. *Energy Proc.* **2014**, *45*, 453−462.

(5) Sreeram, K. J.; Aby, C. P.; Nair, B. U.; Ramasami, T. Colored cool colorants based on rare earth metal ions. *Sol. Energy Mater. Sol. Cells* **2008**, *92*, 1462−1467.

(6) Zhang, Y.; Zhang, Y.; Zhao, X.; Zhang, Y. Sol-gel synthesis and properties of europium-strontium copper silicates blue pigments with high near-infrared reflectance. *Dyes Pigm.* **2016**, *131*, 154−159.

(7) Masui, T.; Takeuchi, N.; Nakado, H.; Imanaka, N. Novel environment-friendly green pigments based on rare earth cuprate. *Dyes Pigm.* **2015**, *113*, 336−340.

(8) George, G.; Vishnu, V. S.; Reddy, M. L. P. The synthesis, characterization and optical properties of silicon and praseodymium

https://doi.org/10.1021/acsomega.2c05748
ACS Omega 2022, 7, 44266−44277

doped Y6MoO12 compounds: Environmentally benign inorganic pigments with high NIR reflectance. *Dyes Pigm.* **2011**, *88*, 109−115.
(9) Han, A.; Ye, M.; Liu, L.; Feng, W.; Zhao, M. Estimating thermal performance of cool coatings colored with high near-infrared reflective inorganic pigments: Iron doped La 2 Mo 2 O 7 compounds. *Energy Build.* **2014**, *84*, 698−703.
(10) Divya, S.; Das, S. Eco-friendly Li3InB2O6 based red pigments for various IR blocking cool coating applications. *Opt. Mater.* **2020**, *109*, 110410.
(11) Pailhé, N.; Gaudon, M.; Demourgues, A. (Ca^{2+}, V^{5+}) co-doped $Y_2Ti_2O_7$ yellow pigment. *Mater. Res. Bull.* **2009**, *44*, 1771−1777.
(12) Calatayud, J. M.; Alarcón, J. V-containing ZrO 2 inorganic yellow nano-pigments prepared by hydrothermal approach. *Dyes Pigm.* **2017**, *146*, 178−188.
(13) Gopal, B.; Muralidharan, A.; Bakthavatsalam, R.; Nellaiappan, S.; Kumar, A. S. Unusual observation of optical property of V 5+ substituted BPO 4 and its tunable redox features. *Mater. Res. Bull.* **2017**, *91*, 122−126.
(14) Lai, H.; Du, Y.; Zhao, M.; Sun, K.; Yang, L. CTAB assisted hydrothermal preparation of YPO4:Tb3+ with controlled morphology, structure and enhanced photoluminescence. *Mater. Sci. Eng., B* **2014**, *179*, 66−70.
(15) Zhang, Y. W.; Yan, Z. G.; You, L. P.; Si, R.; Yan, C. H. General synthesis and characterization of monocrystalline lanthanide orthophosphate nanowires. *Eur. J. Inorg. Chem.* **2003**, 4099−4104.
(16) Yan, Z. G.; Zhang, Y. W.; You, L. P.; Si, R.; Yan, C. H. General synthesis and characterization of monocrystalline 1D-nanomaterials of hexagonal and orthorhombic lanthanide orthophosphate hydrate. *J. Cryst. Growth* **2004**, *262*, 408−414.
(17) Ghosh, P.; de la Rosa, E.; Oliva, J.; Solis, D.; Kar, A.; Patra, A. Influence of surface coating on the upconversion emission properties of LaPO4:Yb/Tm core-shell nanorods. *J. Appl. Phys.* **2009**, *105*, 113532.
(18) Ma, C. G.; Popov, A. V.; Vanetsev, A. S.; Gaitko, O. M.; Orlovskaya, E. O.; Lange, S.; Sildos, Y. V.; Orlovskii, Y. V. Vacuum ultraviolet spectroscopic analysis of Ce3+-doped hexagonal YPO4·0.8H2O based on exchange charge model. *J. Lumin.* **2014**, *152*, 70−74.
(19) Vanetsev, A. S.; Samsonova, E. V.; Gaitko, O. M.; Keevend, K.; Popov, A. V.; Mäeorg, U.; Mändar, Y. V.; Sildos, I.; Orlovskii, Y. V. Phase composition and morphology of nanoparticles of yttrium orthophosphates synthesized by microwave-hydrothermal treatment: the influence of synthetic conditions. *J. Alloys Compd.* **2015**, *639*, 415−421.
(20) Wujczyk, M.; Watras, A.; Szyszka, K.; Wiglusz, R. J. Influence of vanadium concentration on up-conversion luminescence in Er3+-Yb3+ and Tm3+-Yb3+ ions pair co-doped YVxP1−xO4 solid state solution. *J. Alloys Compd.* **2021**, *884*, 161022.
(21) Chanchan, K.; Singh, S. D. Concentration effect on the luminescent and structural properties of YPO4: Eu3+. *Mater. Today: Proc.* **2022**, *65*, 2480−2483.
(22) Minakova, T.; Mjakin, S.; Bakhmetyev, V.; Sychov, M.; Zyatikov, I.; Ekimova, I.; Kozik, I.; Chen, Y.-W.; Kurzina, I. High Efficient YVPO4 Luminescent Materials Activated by Europium. *Crystals* **2019**, *9*, 658.
(23) Zhang, Z.; Zhang, Y.; Feng, F.; Cheng, W.; Xia, X.; Zhang, X. Luminescent properties of Ce3+/Tb3+co-doped glass ceramics containing YPO4 nanocrystals for W-LEDs. *J. Rare Earths* **2016**, *34*, 464−469.
(24) Cao, Y.; Liu, Y.; Feng, H.; Yang, Y. Effects of Bi3+ co-doping on luminescence of YPO4:Dy3+ powders. *Ceram. Int.* **2014**, *40*, 15319−15323.
(25) Angiuli, F.; Cavalli, E.; Boutinaud, P.; Mahiou, R. Emission properties of Sm3+/Bi3+-doped YPO4 phosphors. *J. Lumin.* **2013**, *135*, 239−242.
(26) Elakkiya, V.; Sumathi, S. Effect of preparation methodology on the colour and the NIR reflectance of nickel doped manganese pyrophosphate. *J. Alloys Compd.* **2018**, *768*, 535−544.
(27) Deng, T.; Yan, S.; Hu, J. A novel narrow band UV-B emitting phosphor-YPO4:Sb3+,Gd3+. *J. Rare Earths* **2016**, *34*, 137−142.
(28) Ghosh, D.; Luwang, M. N. Arsenic detection in water: YPO4:Eu3+ nanoparticles. *J. Solid State Chem.* **2015**, *232*, 83−90.
(29) Abid, N.; Khan, A. M.; Shujait, S.; Chaudhary, K.; Ikram, M.; Imran, M.; Haider, M.; Khan, M.; Khan, Q.; Maqbool, M. Synthesis of nanomaterials using various top-down and bottom-up approaches, influencing factors, advantages, and disadvantages: A review. *Adv. Colloid Interface Sci.* **2022**, *300*, 102597.
(30) Di, W.; Zhao, X.; Lu, S.; Wang, X.; Zhao, H. Thermal and photoluminescence properties of hydrated YPO4:Eu3+ nanowires. *J. Solid State Chem.* **2007**, *180*, 2478−2484.
(31) Kahouadji, B.; Guerbous, L.; Jovanović, D. J.; Dramićanin, M. D. Temperature dependence of red emission in YPO4:Pr3+ nanopowders. *J. Lumin.* **2022**, *241*, 118499.
(32) Ding, C.; Tian, M.; Han, A.; Ye, M.; Chen, X. V-doped LaPO4 new solar heat-reflective pigments and its improvement on the aging resistance of poly-methyl methacrylate. *Sol. Energy* **2020**, *195*, 660−669.
(33) Kirankumar, V. S.; Sumathi, S. Catalytic activity of bismuth doped zinc aluminate nanoparticles towards environmental remediation. *Mater. Res. Bull.* **2017**, *93*, 74−82.
(34) Batista, J. C.; de Sousa Filho, P. C.; Serra, O. A. Effect of the vanadium(v) concentration on the spectroscopic properties of nanosized europium-doped yttrium phosphates. *Dalton Trans.* **2012**, *41*, 6310−6318.
(35) Kijkowska, R.; Cholewka, E.; Duszak, B. X-ray diffraction and Ir-absorption characteristics of lanthanide orthophosphates obtained by crystallisation from phosphoric acid solution. *J. Mater. Sci.* **2003**, *38*, 223−228.
(36) Nakamoto, K.*Infrared Spectra of Inorganic and Coordination Compounds*; John Wiley & Sons: New York−London. 328 Seiten, Zahlreiche Abbildungen und Tabellen. Preis: 72s, 1963; Vol. *67*, pp 996.
(37) Luwang, M. N.; Ningthoujam, R. S.; Srivastava, S. K.; Vatsa, R. K. Disappearance and Recovery of Luminescence in Bi3+, Eu3+ Codoped YPO4 Nanoparticles Due to the Presence of Water Molecules Up to 800 °C. *J. Am. Chem. Soc.* **2011**, *133*, 2998−3004.
(38) Azzam, A. B.; El-Sheikh, S. M.; Geioushy, R. A.; Salah, B. A.; El-Dars, M.; Helal, A. S. Facile fabrication of a novel BiPO4 phase junction with enhanced photocatalytic performance towards aniline blue degradation. *RSC Adv.* **2019**, *9*, 17246−17253.
(39) Bouddouch, A.; Amaterz, E.; Bakiz, B.; Guinneton, F.; Taoufyq, A.; Villain, S.; Gavarri, J. R.; Mansori, M.; Valmalette, J. C.; Benlhachemi, A. High photocatalytic performance of bismuth phosphate and corresponding photodegradation mechanism of Rhodamine B. *Res. Chem. Intermed.* **2022**, *48*, 3315−3334.
(40) Kolesnikov, I. E.; Kalinichev, A. A.; Kurochkin, M. A.; Golyeva, E. V.; Terentyeva, A. S.; Kolesnikov, E. Y.; Lähderanta, E. Structural, luminescence and thermometric properties of nanocrystalline YVO4:Dy3+ temperature and concentration series. *Sci. Rep.* **2019**, *9*, 2043.
(41) Wang, W. K.; Wang, S. Y.; Liu, K. F.; Tsai, P. C.; Zhang, Y. H.; Huang, S. Y. Plasma Etching Behavior of SF6 Plasma Pre-Treatment Sputter-Deposited Yttrium Oxide Films. *Coatings* **2020**, *10*, 637.
(42) Parhi, P.; Manivannan, V. Novel microwave initiated solid-state metathesis synthesis and characterization of lanthanide phosphates and vanadates, LMO4 (L=Y, La and M=V, P). *Solid State Sci.* **2008**, *10*, 1012−1019.
(43) Elakkiya, V.; Abhishekram, R.; Sumathi, S. Copper doped nickel aluminate: Synthesis, characterisation, optical and colour properties. *Chin. J. Chem. Eng.* **2019**, *27*, 2596−2605.
(44) Savunthari, K. V.; Shanmugam, S. Effect of co-doping of bismuth, copper and cerium in zinc ferrite on the photocatalytic degradation of bisphenol A. *J. Taiwan Inst. Chem. Eng.* **2019**, *101*, 105−118.
(45) Li, D.; Kaner, R. B. How nucleation affects the aggregation of nanoparticles. *J. Mater. Chem.* **2007**, *17*, 2279−2282.

https://doi.org/10.1021/acsomega.2c05748
ACS Omega 2022, 7, 44266−44277

(46) Rao, P. A.; Raghavendra, V.; Suryanarayana, B.; Paulos, T.; Murali, N.; Varma, P. P.; Chandramouli, K. Cadmium substitution effect on structural, electrical and magnetic properties of Ni-Zn nano ferrites. *Results Phys.* **2020**, *19*, 103487.
(47) Wu, J.; Jia, H.; Li, M.; Jia, H.; Liu, Z. Influence of pH on nano-phosphor YPO_4: 2% Sm^{3+} and luminescent properties. *Appl. Phys. A* **2020**, *126*, 87.
(48) Wang, H.; Odawara, O.; Wada, H. One-step preparation of YVO4:Eu3+ nanoparticles by pulsed laser ablation. *Sci. Rep.* **2016**, *683*, 1−6.
(49) Sameera, S.; Prabhakar Rao, P. P.; James, V.; Divya, S.; Raj, A. K. Influence of (LiLa)1/2MoO4 substitution on the pigmentary properties of BiVO4. *Dyes Pigm.* **2014**, *104*, 41−47.
(50) Pasikatan, M. C.; Steele, J. L.; Spillman, C. K.; Haque, E. Near infrared reflectance spectroscopy for online particle size analysis of powders and ground materials. *J. Near Infrared Spectrosc.* **2001**, *9*, 153−164.
(51) Tao, Z.; Zhang, W.; Huang, Y.; Wei, D.; Seo, H. J. A novel pyrophosphate BaCr2(P2O7)2 as green pigment with high NIR solar reflectance and durable chemical stability. *Solid State Sci.* **2014**, *34*, 78−84.

https://doi.org/10.1021/acsomega.2c05748
ACS Omega 2022, 7, 44266−44277